Electronic Supplementary Information (ESI)

Hollow magnetic Janus microspheres templated from double Pickering emulsions

Yin Ning,[a] Chaoyang Wang,*[a] To Ngai ,*[b] Yu Yang[a] and Zhen Tong[a]

[a] *Research Institute of Materials Science, South China University of Technology, Guangzhou，510640, China*
E-mail: zhywang@scut.edu.cn
[b] *Department of Chemistry, The Chinese University of Hong Kong, Hong Kong, China*
E-mail: tongai@cuhk.edu.hk

Experimental details

Materials: Ferric chloride hexahydrate($FeCl_3 \cdot 6H_2O$), ferrous chloride tetrahydrate($FeCl_2 \cdot 4H_2O$), cetyltrimethylammonium bromide(CTAB), Tetraethoxysilane(TEOS), triethylamine(TEA), HCl, ammonia and ethanol are of analytical grade and used as received without further purification. Styrene (St, Guanghua Chemical Industries Co., China) was distilled under reduced pressure over CaH and 2,2'-azobisisobutyronitrile (AIBN) was recrystallized from ethanol. Both of they were stored in the refrigerator before use. If not otherwise mentioned, all the reagents above are purchased from Shanghai Chemical Reagent Co. (China). The amorphous fumed silica powders (H30) with primary particle diameters quoted of between 5 nm and 30 nm was kindly provided by Wacker Chemie (Burghausen) as a gift. Water used in all experiments was purified by deionization and filtration with a Millipore purification apparatus to the resistivity no less than 18.0 M cm.

Preparation of aqueous Fe_3O_4 dispersion: A mixture of 1.0144 g of $FeCl_3 \cdot 6H_2O$ and 0.3732 g of $FeCl_2 \cdot 4H_2O$ dissolved in 10 ml of water was added to a 50 ml three-necked round bottom flask pre-immersed in an oil bath at 343K and the reaction was allowed to proceed for 2 h after quick droplet-addition of 4 ml 16.5% $NH_3 \cdot H_2O$ under vigorous stirring. The resulting black precipitate was washed with anhydrous ethanol and centrifugalized several times, then re-dispersed in water under ultrasonic treatment and finally the aqueous-Fe_3O_4 dispersion (see Fig. S2 (a)) was obtained after another centrifugation at a high speed of 10000 r/min for 5 min aiming to remove the un-dispersed Fe_3O_4 agglomeration.

Preparation of mesoporous silica nanoparticles (MSNs): MSNs were synthesized applying the method introduced by Möller et al.[1] A stock solution was prepared by mixing 37 ml of water, 5.25 ml of ethanol and 1.4305 g of CTAB, after stirring the above mixture for 15 min at room temperature, 2.06 ml of TEA was added and stirred till totally dissolved. Subsequently, 40 ml of

this stock was charged to a stirrer-equipped flask, which had already immersed in an oil bath at 353 K, thereafter, 2.9 ml TEOS was added dropwisely under vigorous stirring. The mixture was refluxed at 353 K for 2 h and the template extraction was conducted in ethanol/HCl mixture (15 mL HCl/150 mL ethanol) for 30 min in an ice bath under ultrasonic agitation. Mesoporous silica NPs were gained by centrifuging and re-dissolving the sediment in water for several times. At last, the mesoporous silica solution was adjusted to 4 wt. ‰ before use.

Preparation of single and double emulsions: The hydrophobic H30 (ranged from 2 wt. ‰ to 7 wt. ‰, pre-dispersed in organic phase) and hydrophilic MSNs (fixed at 4 wt. ‰, pre-dispersed in water) were adopted as emulsifier to stabilize the single emulsions (W_F-O, inner interface) and double emulsions ((W_F-O)-W, outer interface), respectively. The inner water phase (W_F) of double Pickering emulsion droplets (W_F-O-W) were made of 0~40 mg ml^{-1} of aqueous-Fe_3O_4 dispersion, the middle organic phase consisted of 5 ml of styrene with 1 wt. % AIBN, and outer water phase comprised hydrophilic MSNs of 4 wt. ‰. The single emulsions were produced by ultrasonic and double emulsions were generated by hand-shake.

Polymerization of double emulsions: A permanent magnet was applied and fixed at the desired position to the double emulsions and the thermal polymerization was started by heating the system to 338K for 24 h to complete the polymerization reaction in an oven. The polymerization temperature was chosen at 338K aiming to avoid double emulsions breaking-up. After polymerization reaction, the as-prepared products were washed by ethanol several times, finally dried at 318 K for a couple of days.

Table S1 Data summary of synthetic conditions of microspheres.

Entry No.	Inner water phase (W_F)		Oil phase (O)			W_F/O	Outer water phase (W)		(W_F/O) /W	Magnetic field (Yes/No)
	Fe_3O_4 (mg ml^{-1})	H_2O (ml)	H30 (wt.‰)[a]	AIBN (g)	Styrene (ml)		MSNs (wt.‰)[a]	H_2O (ml)		
1	0	1.25	3	0.05	5	1:4	4	5	1:5	Y
2	10	1.25	3	0.05	5	1:4	4	5	1:5	Y
3	20	1.25	3	0.05	5	1:4	4	5	1:5	Y/N
4	30	1.25	3	0.05	5	1:4	4	5	1:5	Y/N
5	40	1.25	3	0.05	5	1:4	4	5	1:5	Y/N
6	30	1.25	2	0.05	5	1:4	4	5	1:5	Y
7	30	1.25	5	0.05	5	1:4	4	5	1:5	Y
8	30	1.25	7	0.05	5	1:4	4	5	1:5	Y
9	30	1.67	3	0.05	5	1:3	4	5	1:5	Y
10	30	1.00	3	0.05	5	1:5	4	5	1:5	Y

[a] mass fraction of H30 (MSNs) in oil phase (outer water phase)

Instrumentation:

The emulsions were observed with an optical microscope (Carl Zeiss, German), the morphology of microspheres (sliced by a razor blade on a quartz wafer, then sputtered with gold) were surveyed by scanning electron microscopy (SEM) with a Philips XL 30 at the acceleration voltage of 20 kV, and the morphology, size, and pore structure of MSNs were characterized by transmission electron microscopy (JEOL-2100F). The sample in form of ethanol suspension was pipetted on a coated copper grid, dried, and subsequently investigated with an accelerating voltage of 200 kV.

N_2 adsorption/desorption measurements at 77 K were performed on Quantachrome NovaWin2 to study the porosity of the MSNs. The samples were pretreated by out-gassing under vacuum at 423 K. Pore size distributions were obtained by using the BET and BJH model.

The prepared Fe_3O_4 nanoparticles sample was scanned for XRD using a Bruker D8 Advance X-ray diffractometer. Vibrating sample magnetometer (VSM), with an applied field ranging from −30 to +30 kilo-oersted (KOe), was employed to test the magnetic characterizations of the Fe_3O_4 nanoparticles as well as the Janus microspheres at room temperature. The average size and size distribution of the targeted microspheres were determined by laser scattering particle size distribution analyzer (LA-950, Hortiba).

Characterization

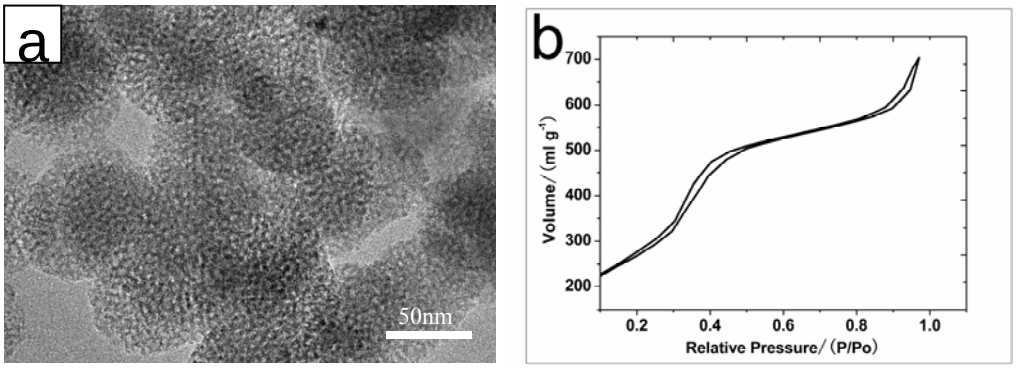

Fig.S1 (a) TEM micrographs of mesoporous silica nanoparticles. (b) N_2 sorption isotherm.

Fig.S1 (a) revealed a well-developed pore structure, which the pores are open, not ordered and oriented from the center to the outer surface, building a complex, worm-like pore system. A type IV isotherm with two closed hysteresis loops typical for mesoporous structures (as shown in Fig. S1 (b)) was observed. At low relative pressure, monolayer adsorption takes place. Thereafter, multilayer adsorption and a strong increase in the adsorption at p/p_o=0.2 shows up, indicating the filling of the meso-pores by capillary condensation. The second noticeable increase in the adsorbed volume occurs at relative pressures above 0.8. The hysteresis loop is caused by inter-particular pores present due to the nanometer-sized particles and by pore blocking or cavitation effects.[2] The BET surface area and the total pore volume were 1088 m^2 g^{-1} and 1.1 ml g^{-1}, respectively. The BJH analysis delivers a narrow nano-pore size distribution with a maximum at 3 nm and no further peaks at higher values which would correspond to larger pore.

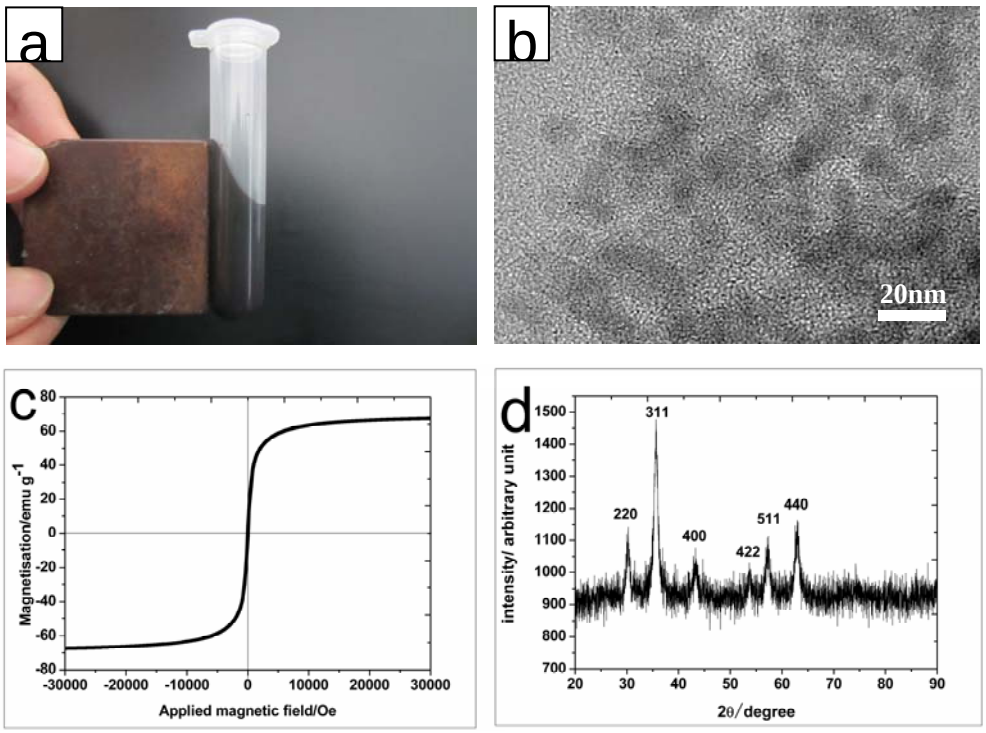

Fig.S2 (a) digital micrographs of aqueous-Fe_3O_4 dispersion with a content of 30 mg ml^{-1}; (b) TEM image of Fe_3O_4 nanoparticles; (c) magnetization curve of Fe_3O_4 nanoparticles; and (d) XRD patterns of as-prepared Fe_3O_4 nanoparticles.

As shown in Fig. S2 (a), well-dispersed Fe_3O_4 nanoparticles aqueous solution contained vessel can be magnetized by a permanent magnet without falling off and phase separation, indicating the stability against agglomeration and strong magnet of aqueous-Fe_3O_4 dispersion. Average diameter of as-prepared Fe_3O_4 nanoparticles was about 10 nm as presented in Fig. S2 (b). The magnetic properties of Fe_3O_4 nanoparticles were investigated with a vibrating sample magnetometer at room temperature. The magnetization curves, as shown in Fig. S2 (c), confirmed the superparamagnetism of Fe_3O_4 nanoparticles with a saturation magnetization values of 67.4 emu g^{-1}. In Fig. S2 (d), XRD patterns revealed diffraction peaks which are characteristic of the Fe_3O_4 crystal with a cubic spinal structure. The diffraction peaks at 2θ=35.62°, 62.9°, 30.24°, 57.26°, and 43.21° can be assigned to (311), (440), (220), (511), and (400) planes of Fe_3O_4 (JCPDS 88-0866), respectively.

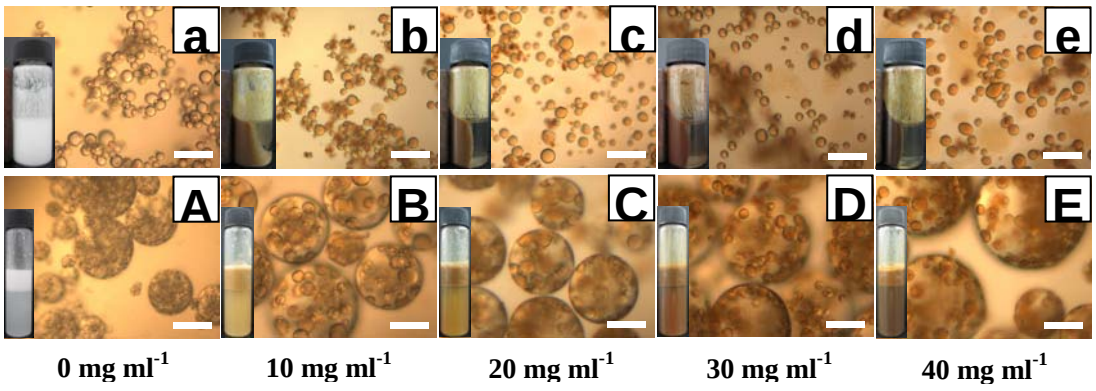

Fig. S3 Effects of Fe_3O_4 concentration on the preparation of emulsions. Each group of vertical micrographs presents W_F/O emulsions and $W_F/O/W$ emulsions at the corresponding Fe_3O_4 concentrations, respectively. The insets of (a)~(e) indicate digital photos of single emulsions being attracted and the insets of (A)~(E) indicate digital photos of double emulsions in absence of magnet. The H30 concentration and volume ratio of W_F/O were fixed at 3 wt. ‰ and 1:4, respectively. All scale bars present 50 μm.

As presented in Fig. S3 (a)~(e), the average size of W_F/O emulsion droplets, which mainly depended on contents of H30 when W_F/O volume ratio fixed at 1:4, was all about 10 μm. The colour of W_F/O emulsions changed from milky-white to brownsh-black with the Fe_3O_4 concentration increased from 0 mg ml^{-1} to 40 mg ml^{-1}. From the comparison of the insets of (a)~(e), the more the Fe_3O_4 concentration was, the easier the W_F/O emulsions can be attracted. However, Fe_3O_4 concentration affected the stability of double emulsions as clean seen from the colour changes of the subnatants, which resulting from breaking-up of double emulsions (see the insets of Fig. S3 (A)~(E)). Therefore, the optimum concentration (30 mg ml^{-1}) was chosen on the consideration of both magnetic ability and emulsions stability.

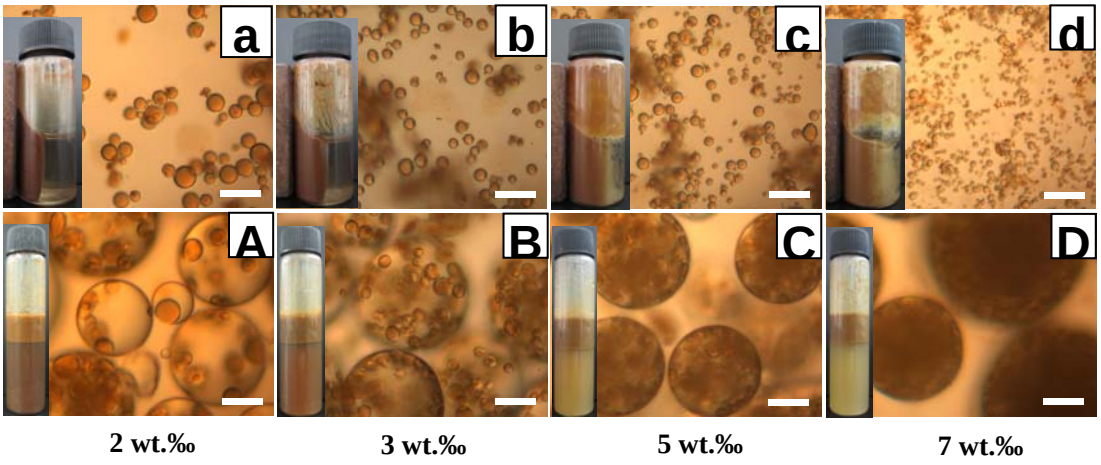

Fig. S4 Effects of H30 concentration on the preparation of emulsions. Each group of vertical micrographs presents W_F/O emulsions and $W_F/O/W$ emulsions at the corresponding H30 concentrations, respectively. The insets of (a)~(d) indicate digital photos of single emulsions being attracted and the insets of (A)~(D) indicate digital photos of double emulsions in absence of magnet. The Fe_3O_4 concentration and volume ratio of W_F/O were fixed at 30 mg ml^{-1} and 1:4, respectively. All scale bars present 50 μm.

The average diameter of W_F/O emulsions decreased from 15 μm to 2 μm with the H30 content increased from 2 wt. ‰ to 7 wt. ‰, as seen from Fig. S4 (a)~(d). Meanwhile, the W_F/O emulsions became immagneticable when H30 content gets higher due to the increasing viscosity (see the insets of (a)~(d)). As shown in Fig. S4 (A)~(D), both the distribution of W_F/O droplets in double emulsions and the stability of double emulsions got better when H30 concentration was increased. So, in this situation, the optimum content of H30 was chosen at 3 wt. ‰.

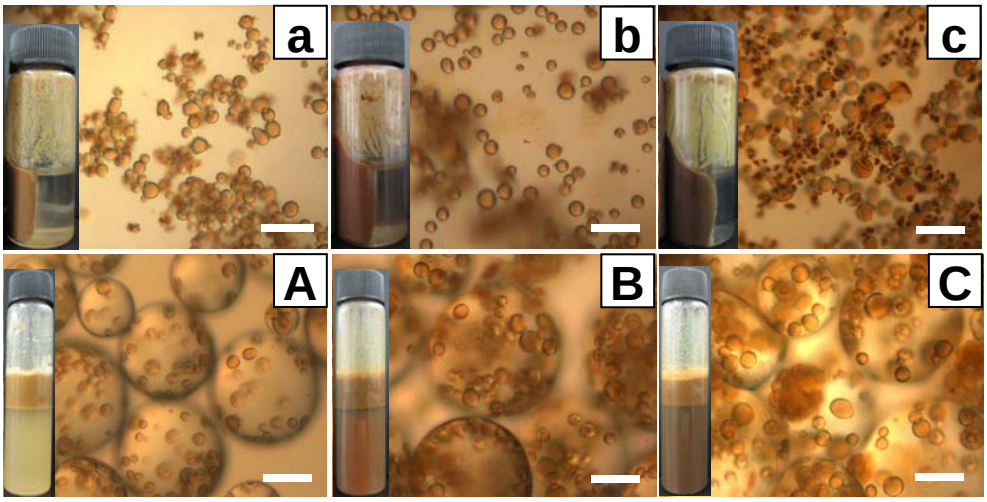

Fig. S5 Effects of volume ratios of inner water phase (W_F) to middle oil phase (O) on the preparation of emulsions. Each group of vertical micrographs presents W_F/O emulsions and $W_F/O/W$ emulsions at the corresponding volume ratios, respectively. The insets of (a)~(c) indicate digital photos of single emulsions being attracted and the insets of (A)~(C) indicate digital photos of double emulsions in absence of magnet. The Fe_3O_4 concentration and H30 content were fixed at 30 mg ml^{-1} and 3 wt. ‰, respectively. All scale bars present 50 μm.

As expected, the colour of W_F/O emulsions became darker even the Fe_3O_4 concentration was fixed at 30 mg ml^{-1} (shown in Fig. S5). That is because changes in the volume ratio of W_F/O indirectly altered the relative content of H30. Agglutinations were observed in Fig. S5 (c) and (C), indicating the breaking-up of emulsions owing to the low H30 content. Note that single emulsion droplets were just half-assembled in the glass bottle in the presence of external magnet when Fe_3O_4 concentration, H30 content, and W_F/O volume ratio fixed at 30 mg ml^{-1}, 3 wt. ‰, and 1:4, respectively. It is well agree with the half-concentration of multihollow structure within the Janus microsphere.

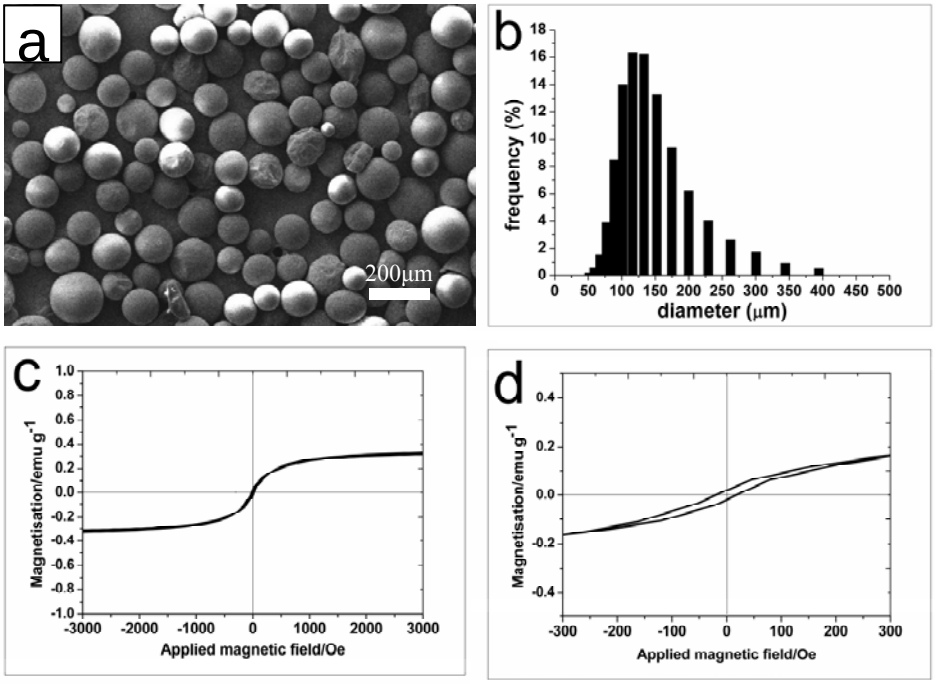

Fig. S6 (a) SEM image of Janus microspheres; (b) Sizes and size distributions of Janus microspheres; (c) Magnetization curve of as-prepared Janus microspheres at 298 K; (d) Hysteresis loop near the zero magnetic field region. All these datas were gained from the sample of Entry No.4 listed in Table 1.

As shown in Fig. S6 (a) and (b), the sizes of Janus microspheres mainly ranged from 80 μm to 150 μm, resulting from the preparation method. It is believed that well-size distribution can be obtained if microfluidic technology was applied. Fig. S6 (c) and (d) presented the magnetisation curve of Janus microspheres at room temperature. From these two graphs, we found that the saturation magnetisation (M_S), the remanence magnetisation (Mr) and the coercivity (Hc) for this sample are 0.32 emu g^{-1}, 0.18 emu g^{-1} and 31.50 Oe, respectively.

References

[1] K. Möller, J. Kobler and T. Bein, Adv. *Funct. Mater.*, 2007, ***17***, 611.
[2] M. Thommes, B. Smarsly, M. Groenewolt, P. I. Ravikovitch and A. V. Neimark, *Langmuir*, 2005, ***22***, 756.